Evaluation of Stainless Steel Pipe Cracking: Causes and Fixes*

by

W. J. Shack, T. F. Kassner, P. S. Maiya, F. A. Nichols,
J. Y. Park, and W. Ruther

Argonne National Laboratory
9700 South Cass Avenue
Argonne, Illinois 60439

Materials Science and Technology Division

October 1983

To be presented at the 11th Water Reactor Safety Research Information Meeting, October 24-28, 1983, National Bureau of Standards (NBS), Gaithersburg, MD.

*Work supported by the Office of Nuclear Regulatory Research, U.S. Nuclear Regulatory Commission.

Evaluation of Stainless Steel Pipe Cracking: Causes and Fixes

by

W. J. Shack, T. F. Kassner, P. S. Maiya, F. A. Nichols,
J. Y. Park, and W. Ruther

Materials Science and Technology Division
Argonne National Laboratory
Argonne, Illinois 60439

E. F. Rybicki

E. F. Rybicki, Inc.

INTRODUCTION

Leaks and cracks in the heat-affected zones of weldments in austenitic stainless steel piping and associated components of boiling water reactors (BWRs) have been observed since the mid-1960s. Since that time, cracking has continued to occur and indications have been found in all parts of the recirculation system, including the largest diameter lines.

Proposed solutions include remedies primarily intended to produce a more favorable residual stress state, materials which are more resistant to stress corrosion cracking (SCC), and changes in the reactor environment which decrease the susceptibility to cracking. In addition to evaluating these remedies, it is also important to gain a better understanding of key variables such as residual stresses, crack growth rates, and the leak-before-break margin in flawed piping, which may impact regulatory decisions on operating plants.

TECHNICAL PROGRESS

The main areas of effort during the past year have been (1) studies of impurity effects on susceptibility to intergranular stress corrosion cracking (IGSCC), (2) crack growth rate measurements, (3) finite-element studies of residual stress produced by induction heating stress improvement (IHSI) and the addition of weld overlays to flawed piping, (4) leak-before-break analyses of piping with 360° part-through cracks, and (5) parametric studies on the effect of through-wall residual stresses on IGSCC crack growth behavior in large-diameter piping weldments. ANL efforts on acoustic leak detection and nondestructive evaluation are reported elsewhere in these Proceedings by D. S. Kupperman et al.[1]

The study of impurity effects on IGSCC is important both for a better understanding of the susceptibility and crack growth rates of conventional austenitic stainless steels in typical BWR environments and for an assessment of

---

*Work supported by the Office of Nuclear Regulatory Research, U.S. Nuclear Regulatory Commission.

the effectiveness of proposed long-term solutions such as addition of hydrogen to the feedwater and the use of Type 316NG (nuclear grade) extra-low-carbon, nitrogen-strengthened steels.

Constant Extension Rate Tensile (CERT) Experiments

CERT experiments have been conducted on several heats of austenitic stainless steel to determine the influence of water chemistry, degree of sensitization, strain rate, and material composition on the SCC susceptibility and the mode of crack propagation in the steels.

With regard to the influence of the reactor coolant environment, our results show a strong synergistic effect of dissolved oxygen (produced by radiolytic decomposition of the water in the reactor) and impurities (e.g., H_2SO_4 and NaCl from decomposition of ion exchange resins and condenser leakage, respectively) on the IGSCC susceptibility and cyclic crack growth properties of the steels. The influence of dissolved oxygen and sulfate (as H_2SO_4) concentrations on the time to failure of lightly and moderately sensitized Type 304 stainless steel (heat 30956) in 289°C water is shown in Fig. 1. A sulfate concentration of 0.1 ppm, which is within the normal operating limits for conductivity (<1.0 μS/cm at 25°C) and pH (5.6 to 8.6 at 25°C) of reactor coolant water, produces a large increase in IGSCC susceptibility (i.e., a significant decrease in the time to failure) of Type 304 SS for dissolved oxygen concentrations $\gtrsim$0.1 ppm. Based on these results, it was not clear whether the potential benefits associated with small additions of hydrogen to the reactor feedwater could be realized in the presence of low levels of impurities. Additional information in Fig. 2 reveals that at low dissolved oxygen concentrations, viz., ~0.03 and 0.005 ppm (upper curve of each panel), which are representative of an alternative BWR water chemistry produced by adding ~1.5 ppm hydrogen to the feedwater, the sulfuric acid has a small effect on IGSCC susceptibility for a conductivity of $\lesssim$1 μS/cm. However, for the normal dissolved oxygen concentrations of ~0.2 ppm (lower curve of each panel), sulfuric acid produces a marked decrease in the time to failure even with ~0.5 ppm dissolved hydrogen. In the reactor core and recirculation system, the dissolved oxygen and hydrogen levels are coupled through radiolysis of the water, which occurs in the core, whereas in the laboratory the concentration of each species was altered independently. The results in Fig. 2 indicate that hydrogen itself plays a relatively minor role in the SCC susceptibility relative to the dissolved oxygen concentration.

During the CERT experiments, the electrochemical potentials of Type 304 stainless steel and a platinum electrode were monitored as a function of time. The potential measurements were made at 289°C relative to an external 0.1M KCl/AgCl/Ag reference electrode and the values were converted to the standard hydrogen electrode at 289°C. From the standpoint of delineating the influence of the high-temperature water on IGSCC susceptibility of Type 304 stainless steel, the corrosion potential of the steel is primarily a function of the dissolved oxygen concentration whereas the conductivity is directly related to the concentration of ionic impurities in the water. The regime of corrosion potential and conductivity in which Type 304 stainless steel is immune to IGSCC at 289°C, based upon the CERT results at a strain rate of 1×10^{-6} s^{-1}, is shown in Fig. 3. In classifying fracture mode, a fracture morphology with both transgranular (TG) and intergranular (IG) regions was considered to be

intergranular. It is clear from these results that at both levels of sensitization, the steel is susceptible to IGSCC at 289°C in very pure water ($\lesssim$0.1 μS/cm) at corrosion potentials $\gtrsim$50 mV (SHE). Water purity is still an important factor in IGSCC at a corrosion potential of -350 mV (SHE); i.e., the conductivity must be $\lesssim$0.2 μS/cm to achieve immunity to IGSCC. A corrosion potential of -350 mV (SHE) was obtained for Type 304 SS in the Dresden-2 reactor during hydrogen addition to the feedwater,[2] which suppressed the oxygen concentration of the water in the recirculation loop to $\lesssim$20 ppb. Based on the fracture surface morphology of CERT specimens tested in 289°C water, other studies[3] suggest an even greater role of impurities at low oxygen levels. It is important to note that the results in Fig. 3 are based on one impurity (sulfate) and one strain rate (1×10^{-6} s^{-1}). Additional information will be obtained at lower strain rates to establish the position of the curves for low dissolved oxygen concentrations and potentials. The influence of other impurities must also be investigated before we can specify realistic impurity levels (which may depend on the nature of the impurity) for which hydrogen additions will give significant reductions in susceptibility to IGSCC.

With regard to the influence of different impurities on the CERT parameters of Type 304 SS (Heat No. 53319) at a higher dissolved oxygen concentration (0.2 ppm), sulfate may be somewhat more detrimental than chloride at a concentration of 0.1 ppm. Under current specifications for reactor water purity, chloride levels are closely monitored, but no explicit measurements of sulfate are normally made.

The effect of pH on IGSCC has been examined in a series of tests in which the sulfate concentration was held fixed while the pH was varied by changing the proportions of sulfuric acid and sodium sulfate in the solution. The results, shown in Fig. 4, indicate that pH per se has relatively little effect on the aggressiveness of the environment, although there is a slight tendency for the less acidic solutions to be more detrimental. (Similar results have been obtained for HCl and NaCl.)

Initial results on the influence of various cations in dilute sulfate solutions on IGSCC susceptibility of sensitized Type 304 SS in 289°C water are shown in Table I. In the presence of $\sim$0.2 ppm dissolved oxygen, the addition of any sulfate compound at the 0.1-ppm sulfate level markedly increases the susceptibility. For this anion, the choice of cation (with the exception of H^+, which is least deleterious) seems to have a secondary effect on the CERT parameters.

Impurity effects on the SCC susceptibility of Types 316 and 316NG stainless steel have also been evaluated in CERT experiments at 289°C. The average crack growth rates for these materials are plotted in Figs. 5 and 6 as a function of strain rate for tests in oxygenated water containing 0.5 ppm chloride and 0.1 ppm sulfate, respectively, added as acid. After realistic heat treatments, Type 316NG is extremely resistant to IGSCC even in impurity environments. However, as shown in Fig. 6, TGSCC has been observed in BWR-quality water (0.2 ppm dissolved oxygen, 0.1 ppm sulfate) at low strain rates ($<10^{-7}$ s^{-1}). It is not yet clear whether the nuclear-grade material is any more susceptible to TGSCC than solution-annealed conventional austenitic stainless steels, for which the service experience with TGSCC has been relatively satisfactory. (Under similar environmental and loading conditions, sensitized stainless steels crack

intergranularly.) However, data for both BWR conditions (Fig. 6) and for somewhat more aggressive environments (Fig. 5) suggest that even when transgranular cracking does occur in Type 316NG, the transgranular crack growth rates are approximately an order of magnitude less than the intergranular crack growth rates for sensitized conventional stainless steels under the same loading and environmental conditions.

Crack Growth Rate Measurements on Fracture Mechanics Specimens

Most of the IGSCC crack growth rate data currently available are for constant load histories. In reality, small load fluctuations will occur in-reactor, and these could have an effect on crack growth rates. To simulate these small load fluctuations, a number of tests (Table II) have been performed at high load ratios, R, ranging from 0.94 to 0.95. The effect of the fluctuating load on crack growth rate seems to vary from one heat of Type 304 stainless steel to another. For heat 10285 at two different levels of sensitization, there is little difference in crack growth rates for constant loads and a small fluctuating load with f = 0.1 Hz and R = 0.95. However, for heat 30956 with $K_{max} \leq 38$ MPa·m$^{\frac{1}{2}}$, crack growth rates differ by almost an order of magnitude between tests at ∿0.1 Hz and those at ∿0.01-0.001 Hz. Attempts to correlate the effects of different load ratios and frequencies on crack growth rates in terms of a crack-tip strain rate based on linear elastic fracture mechanics (LEFM) were not successful. There appears to be a strong heat-to-heat variation in the effect of degree of sensitization (DOS) on susceptibility to IGSCC and crack growth rate, both in terms of the threshold level of sensitization needed to produce susceptibility and in the effect of varying DOS on crack growth rates.

The relative IGSCC susceptibility observed in CERT tests for Type 304 stainless steel (heat 30956) with different levels of sensitization in high-purity oxygenated water (8 ppm O_2) and in simulated BWR-quality water with 0.2 ppm oxygen and 0.1 ppm sulfate as H_2SO_4 has been confirmed in cyclic-crack-growth experiments with a positive sawtooth waveform at a load ratio of 0.95, K_{max} of 28 MPa·m$^{\frac{1}{2}}$, and frequency of 8 x 10^{-2} Hz. The results are shown in Figs. 7 and 8 for the respective environments. The moderately sensitized material (EPR = 20 C/cm^2) exhibits the highest crack growth rate in oxygenated water (2.7 x 10^{-3} mm h^{-1}), whereas in the impurity environment containing 0.2 ppm dissolved oxygen and 0.1 ppm sulfate, the lightly sensitized material (EPR = 2 C/cm^2) cracks at a higher rate (3.6 x 10^{-4} mm h^{-1}). Crack growth did not occur in the solution-annealed steel in either environment for the above loading conditions.

Residual Stress Associated with IHSI and Weld Overlays

Residual stress improvement remedies such as IHSI and weld overlay techniques have been proposed as both long- and short-term remedies. A reasonably convincing case can be made for the effectiveness of these types of remedies when they are applied to unflawed weldments. However, their effectiveness when applied to weldments with flaws is less clear. Detailed finite-element calculations of the stress state at crack tips for weldments subjected to IHSI and weld overlay repairs have been carried out under subcontract with E. F. Rybicki, Inc. In the case of IHSI, calculations were performed for a preexisting ∿8%-throughwall flaw, illustrative of a flaw that

might be missed during an in-service inspection. The stress state ahead of the crack tip under an applied load of 103 MPa (15 ksi) is shown in Fig. 9. Without IHSI, extremely high stresses (~310 MPa or 45 ksi) are present ahead of the crack tip; with IHSI, the stresses under this rather high applied load are not compressive, but they are quite low [<35 MPa (5 ksi)].

For the weld overlay case, a deeper (~20%-throughwall) crack was assumed. The stresses ahead of the crack tip under an applied load of 103 MPa (15 ksi) are shown in Fig. 10. Even under this applied load, the crack tip is under a highly compressive residual stress field; thus, the overlay procedure appears even more effective than IHSI in inducing compressive residual stress fields. Additional calculations are being carried out to determine the stress state associated with deeper (~50%-throughwall) cracks. In a cooperative effort with NUTECH, experimental measurements of throughwall residual stresses in weldments with weld overlays are being carried out to benchmark the finite-element analyses.

Leak-Before-Break Analysis

In addition to assessing the effectiveness of possible remedies for IGSCC, it is also important to consider the general characteristics of IGSCC in BWR piping systems and the failure behavior of these systems. The inherent toughness of Type 304 stainless steel assures a large leak-before-break margin for simple throughwall cracks. However, IGSCC in large-diameter weldments is characterized by large aspect ratios, and one must consider the possibility that a 360° crack will occur before a localized throughwall crack develops. The results of a leak-before-break analysis for this situation are shown in Figs. 11 and 12. Failure is described in terms of a critical net-section stress. Upper and lower bounds for the length of a throughwall crack necessary to produce 5-gal/min leakage have been estimated using a two-phase flow model and estimates of the frictional losses within an intergranular crack based on experiments at Argonne and Battelle (4). For a simple throughwall crack (i.e., when the fractional depth of the 360° crack is zero), there is a significant leak-before-break margin even for the upper-bound estimate of the crack length required for detectable leakage. The analysis suggests that the leak-before-break margin is violated only in the case of very deep, long cracks, and that for relatively shallow (<25%-throughwall) circumferential cracks the margin is still substantial.

The analysis of IGSCC growth using LEFM suggests that the throughwall distribution of residual stress plays an important role in determining the nature of the crack growth. Most of the available experimental data on throughwall residual stresses in large-diameter pipe weldments[5] are summarized in Fig. 13, along with various analytical representations that roughly bound the data and give an "average" distribution. In all cases the residual stresses are tensile on the inner surface of the weldment and then become compressive a relatively short distance into the wall. LEFM calculations of the maximum depth to which IGSCC could grow are shown as a function of the external applied stress in Fig. 14 for the three analytical representations of the residual stresses shown in Fig. 13. These results suggest that in many cases the cracks may arrest and not grow completely through the wall, but the actual depth the crack may reach is a sensitive function of the residual stress distribution and the

applied stress. Small changes in the applied stress produce marked increases in the maximum depth of the crack. As Fig. 15 shows, the accelerated throughwall crack growth occurs relatively quickly after a longer period of relatively slow growth.

Future Work

The work to assess the effect of impurities on SCC in both conventional BWR environments and the low-oxygen environment characteristic of BWRs with hydrogen additions will continue. Additional impurities (both cations and anions) will be evaluated based upon recent analyses of reactor coolant water by ion chromatography and ion-exchange separation techniques coupled with conductivity or photometric measurements. The effect of strain rate will be evaluated further, and fracture mechanics crack growth experiments will be continued to verify the results and quantify the degree of improvement/degradation. Confirmatory tests in impurity environments will also be carried out on the other materials used in the reactor coolant boundary and critical internal components. The study of the effect of impurities on the susceptibility of Type 316NG stainless steel to SCC will continue. Low-stress cyclic pipe tests will be carried out to assess the effect of impurities on the apparent factor of improvement. Long-term aging studies on Types 316NG and 304 stainless steel will also continue.

References

1. D. S. Kupperman, T. N. Claytor, and R. Groenwald, "Leak Detection and Ultrasonic Crack Detection," these Proceedings.

2. E. L. Burley, "Oxygen Suppression in Boiling Water Reactors-Phase 2," Final Report, DOE/ET/34203-47, NEDC-23856-7 (October 1982).

3. W. Childs et al., "Plant Materials Program: Progress June 1981 to May 1982," EPRI NP-2879-SR, Electric Power Research Institute (February 1983).

4. R. Collier et al., "Study of Critical Two-Phase Flow Through Intergranular Stress Corrosion Cracks," Draft Report to the Electric Power Research Institute, to be published by Battelle Columbus Laboratories.

5. R. Horn et al., "The Growth and Stability of Stress Corrosion Cracks in Large Diameter BWR Piping," EPRI-NP-2472, Vol. 2, Electric Power Research Institute (1982).

TABLE I. Influence of 0.1 ppm Sulfate with Different Cations on the IGSCC Susceptibility of Lightly Sensitized (EPR = 2 C/cm^2) Type 304 SS at 289°C in Water Containing ∿0.2 ppm Dissolved Oxygen[a]

Feedwater				CERT Parameters	
Oxygen (ppm)	Impurity Species	Cond. at 25°C (μS/cm)	pH at 25°C	Failure Time (h)	Maximum Stress (MPa)
0.20	H_2SO_4	0.91	5.74	79	402
0.20	Na_2SO_4	0.66	6.90	54	345
0.24	$(NH_4)_2SO_4$	0.43	6.27	54	307
0.25	$FeSO_4$	0.55	6.11	58	324
0.25	$Cr_2(SO_4)_3$	0.59	5.95	47	307
0.25	$NiSO_4$	0.37	6.26	49	315
0.26	$CuSO_4$	0.44	6.22	56	330
0.26	$ZnSO_4$	0.39	6.13	55	347
0.28	$Al_2(SO_4)_3$	0.73	5.73	40	281

[a]Specimens were exposed to the environment for ∿20 h at 289°C before straining at a rate of 1×10^{-6} s^{-1}.

TABLE II. Effects of Loading History and Degree of Sensitization on Crack Growth Rates in Type 304 Stainless Steel Tested in 288°C Water with 8 ppm O_2

EPR (C/cm^2)	f (Hz)	Load Ratio, R	K_{max} ($MPa \cdot m^{\frac{1}{2}}$)	å(m/s)
		Heat 10285		
4	0	1	33-34	1.2×10^{-10}
↓	2×10^{-3}	0.5	30-33	3.4×10^{-9}
	2×10^{-3}	0.6	32-33	6.6×10^{-10}
	2×10^{-3}	0.7	30-31	3.4×10^{-10}
	2×10^{-3}	0.7	32-33	5.9×10^{-10}
	2×10^{-3}	0.8	30-32	7.4×10^{-10}
	1×10^{-1}	0.94	30-31	3.1×10^{-10}
↓	1×10^{-1}	0.94	31-32	1.9×10^{-10}
15	0	1	32-33	2.2×10^{-10}
↓	2×10^{-3}	0.5	30-32	2.8×10^{-9}
	2×10^{-3}	0.6	28-29	5.6×10^{-10}
↓	1×10^{-1}	0.94	30	2.1×10^{-10}
		Heat 30956		
20	8×10^{-2}	0.95	28	7.5×10^{-10}
↓	↓	↓	34	1.0×10^{-9}
			35	1.2×10^{-9}
	8×10^{-3}		34	1.2×10^{-10}
	↓		38	1.5×10^{-10}
			50	4.7×10^{-10}
			61	1.1×10^{-9}
			64	1.7×10^{-9}
	8×10^{-4}		28	1.2×10^{-10}
	↓		67	1.9×10^{-9}
			70	3.2×10^{-8}
↓	↓	↓	72	3.3×10^{-8}

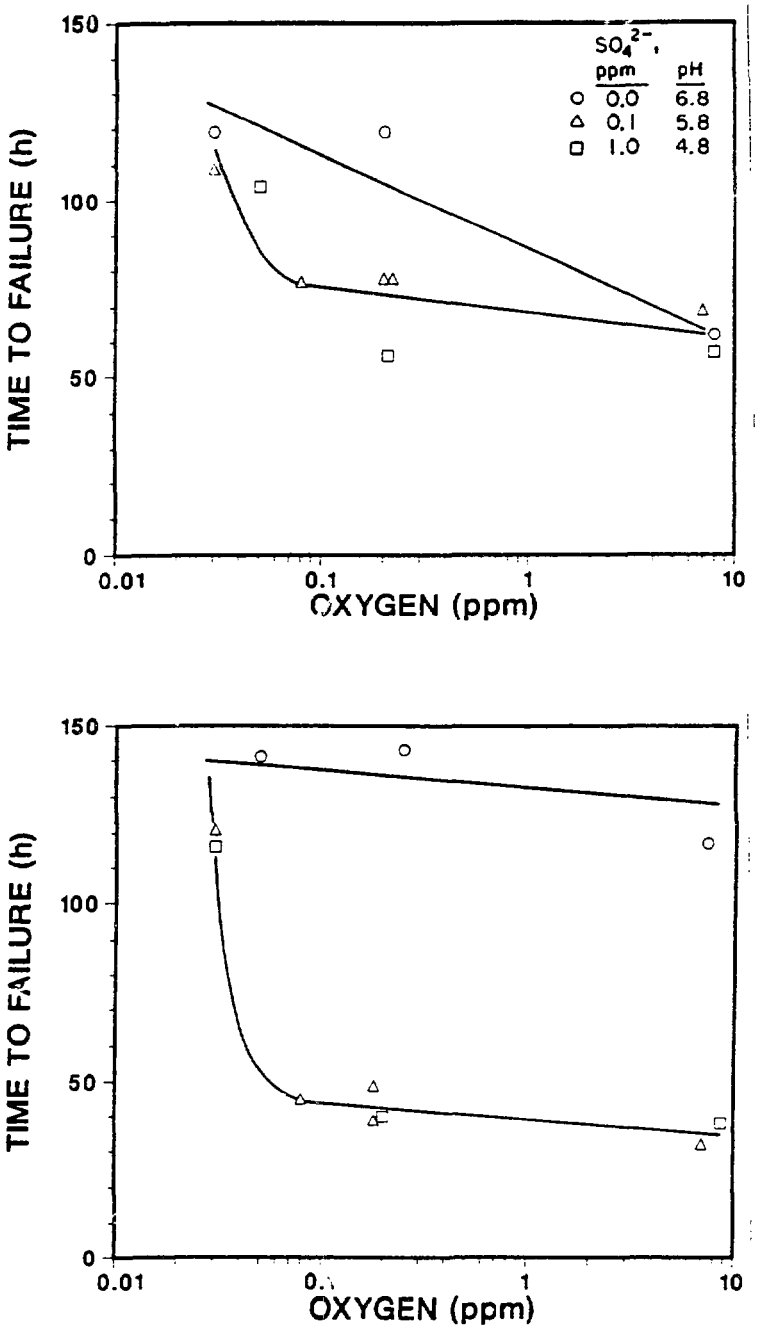

Fig. 1. Effect of Dissolved Oxygen and Sulfate (as H_2SO_4) Concentration in 289°C Water on the Time to Failure of Lightly (EPR = 2 C/cm^2) and Moderately (EPR = 20 C/cm^2) Sensitized Type 304 SS (Heat 30956) in CERT Experiments at a Strain Rate of 1 x 10^{-6} s^{-1}.

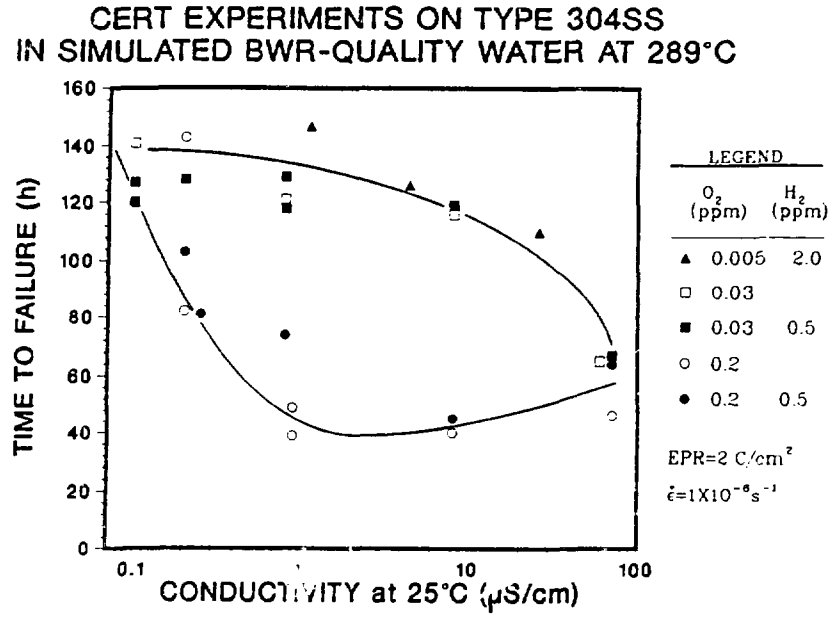

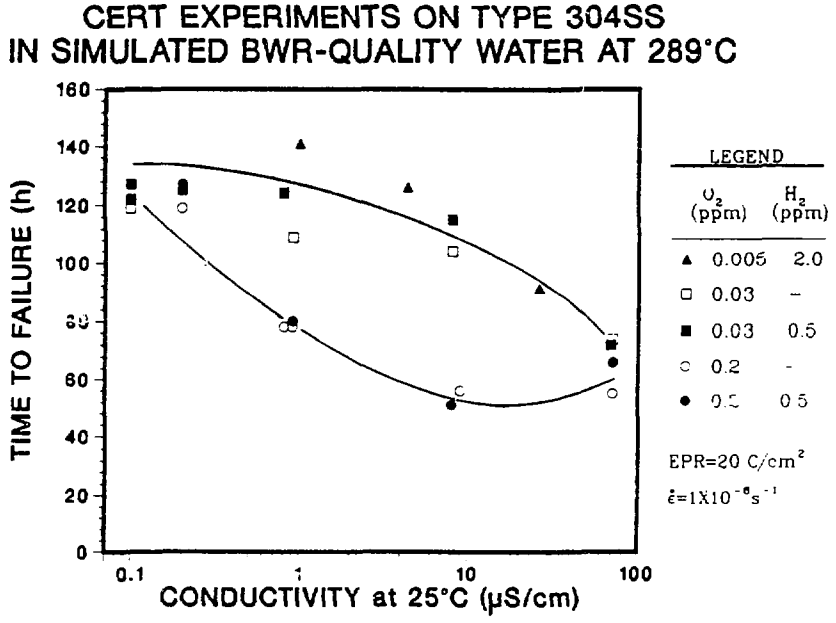

Fig. 2. Influence of Conductivity of the Feedwater on the Time to Failure of Lightly (EPR = 2 C/cm^2) and Moderately (EPR = 20 C/cm^2) Sensitized Type 304 SS (Heat 30956) in CERT Experiments at 289°C and a Strain Rate of 1 x 10^{-6} s^{-1} in Water Containing 0.2, 0.03, and 0.005 ppm Dissolved Oxygen Without (Open Symbols) and With (Closed Symbols) 0.5 or 2.0 ppm Hydrogen.

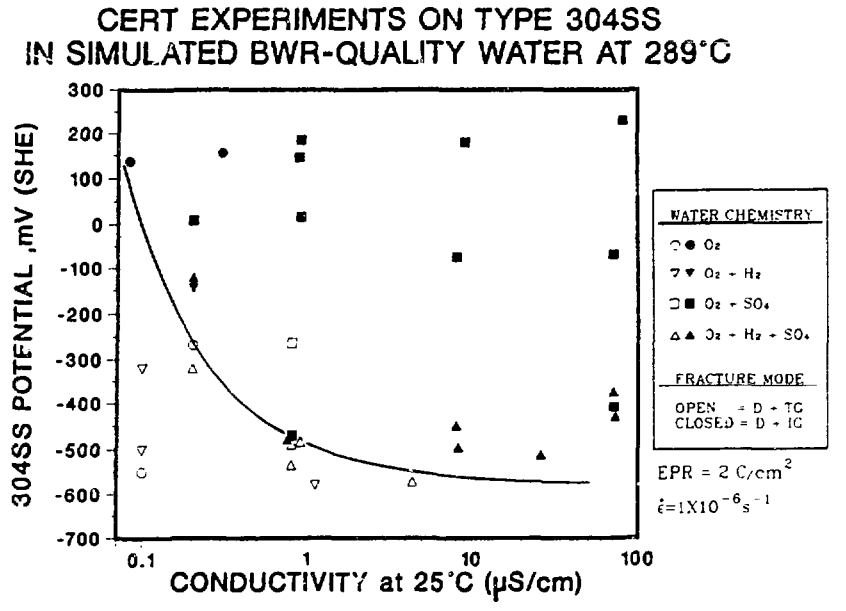

(a)

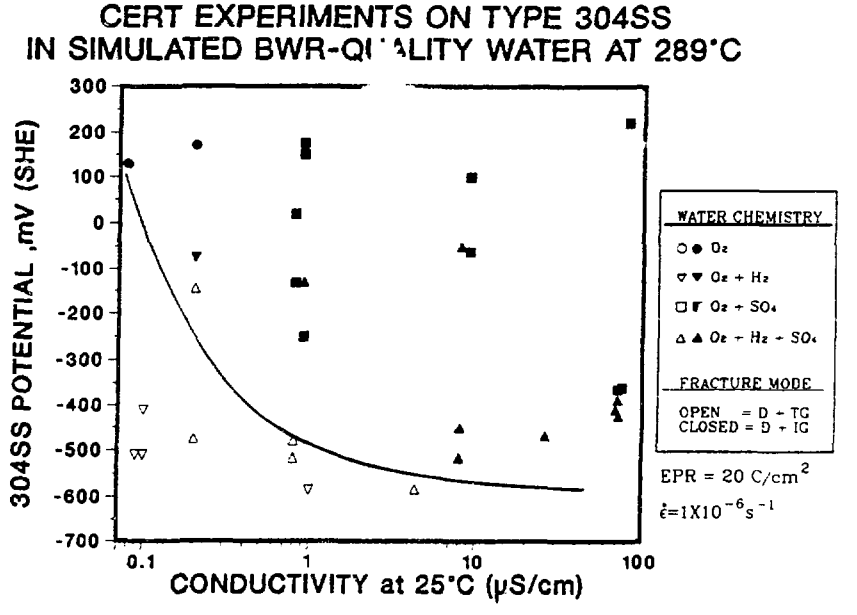

(b)

Fig. 3. Regime of Corrosion Potential and Feedwater Conductivity that Results in Immunity to IGSCC (Region Below Curve in Each Panel) for (a) Lightly (EPR = 2 C/cm^2) and (b) Moderately (EPR = 20 C/cm^2) Sensitized Type 304 SS in CERT Experiments at 289°C in Simulated BWR-Quality Water Containing Dissolved Oxygen, Hydrogen, and Sulfate as H_2SO_4. Open and closed symbols represent transgranular and intergranular fracture mode, respectively.

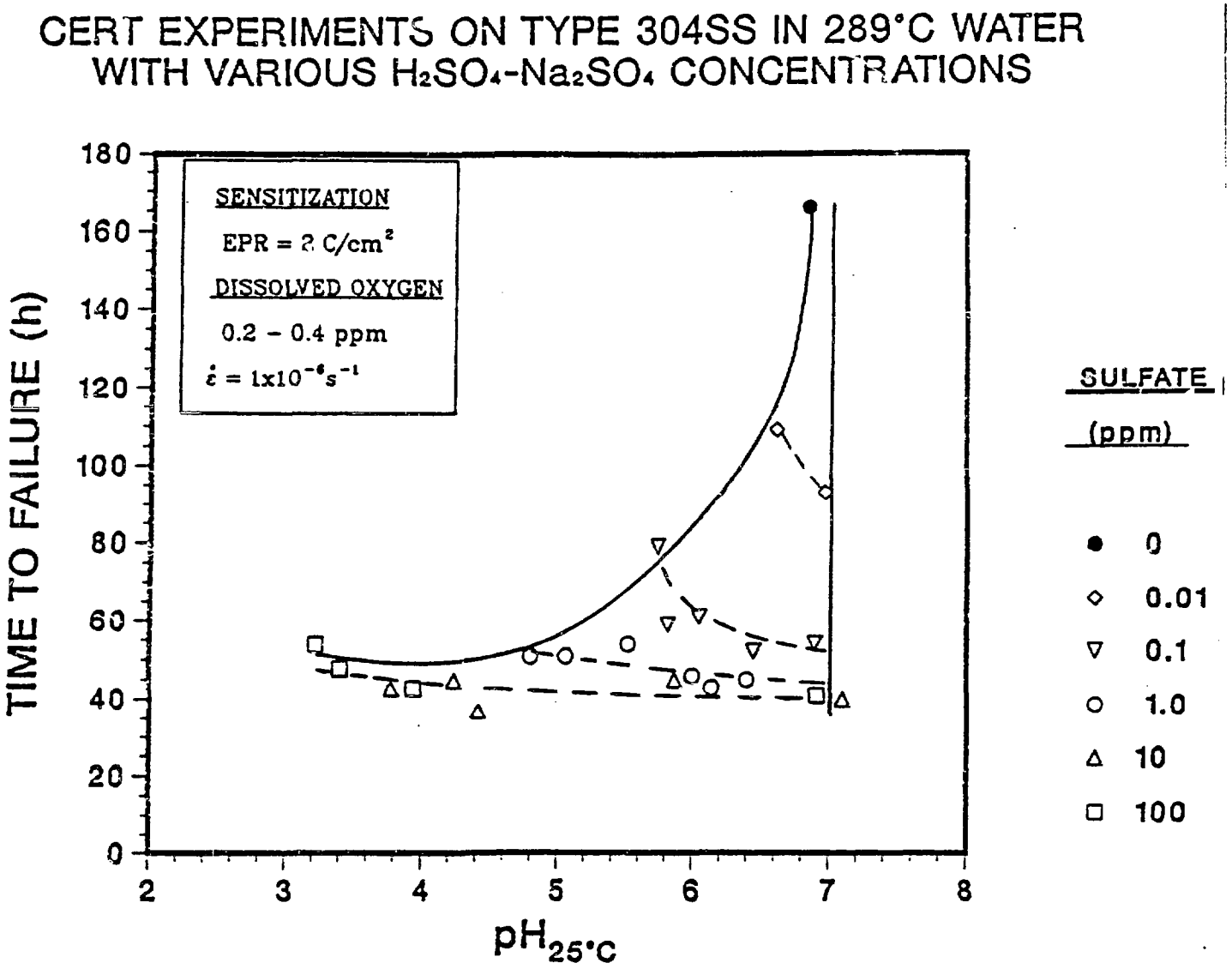

Fig. 4. Effect of pH of H_2SO_4-Na_2SO_4 Solution, at Several Total Sulfate Concentrations, on the Time to Failure of Lightly Sensitized (EPR = 2 C/cm^2) Type 304 SS Specimens in CERT Experiments at a Strain Rate of 1 x 10^{-6} s^{-1} in 289°C Water with 0.2-0.4 ppm Dissolved Oxygen.

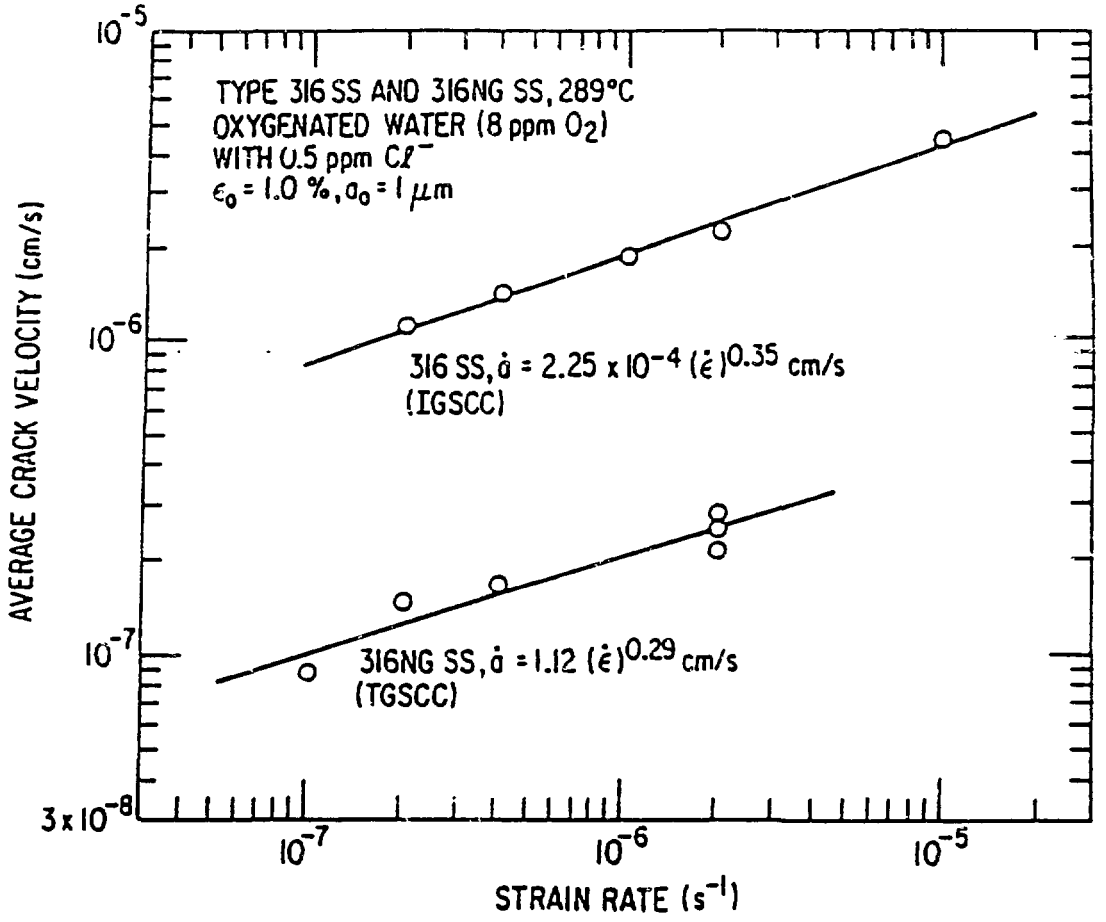

Fig. 5. Average Crack Growth Rates of Types 316NG and 316 SS in Oxygenated Water (8 ppm O_2) with 0.5 ppm Cl^-, as a Function of Strain Rate.

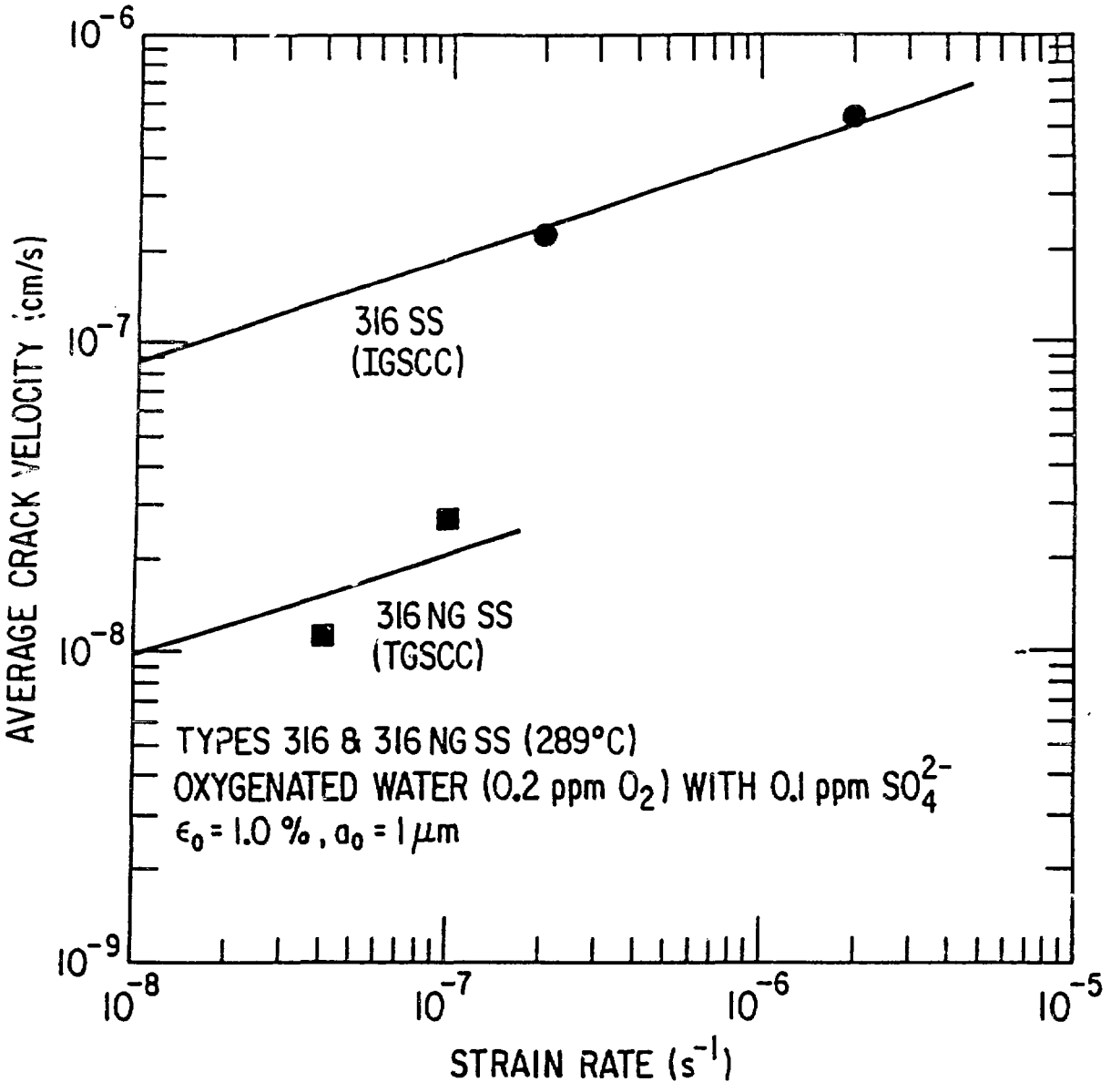

Fig. 6. Average Crack Growth Rates of Types 316NG and 316 SS in Oxygenated Water (0.2 ppm O_2) with 0.1 ppm SO_4^{2-}, as a Function of Strain Rate.

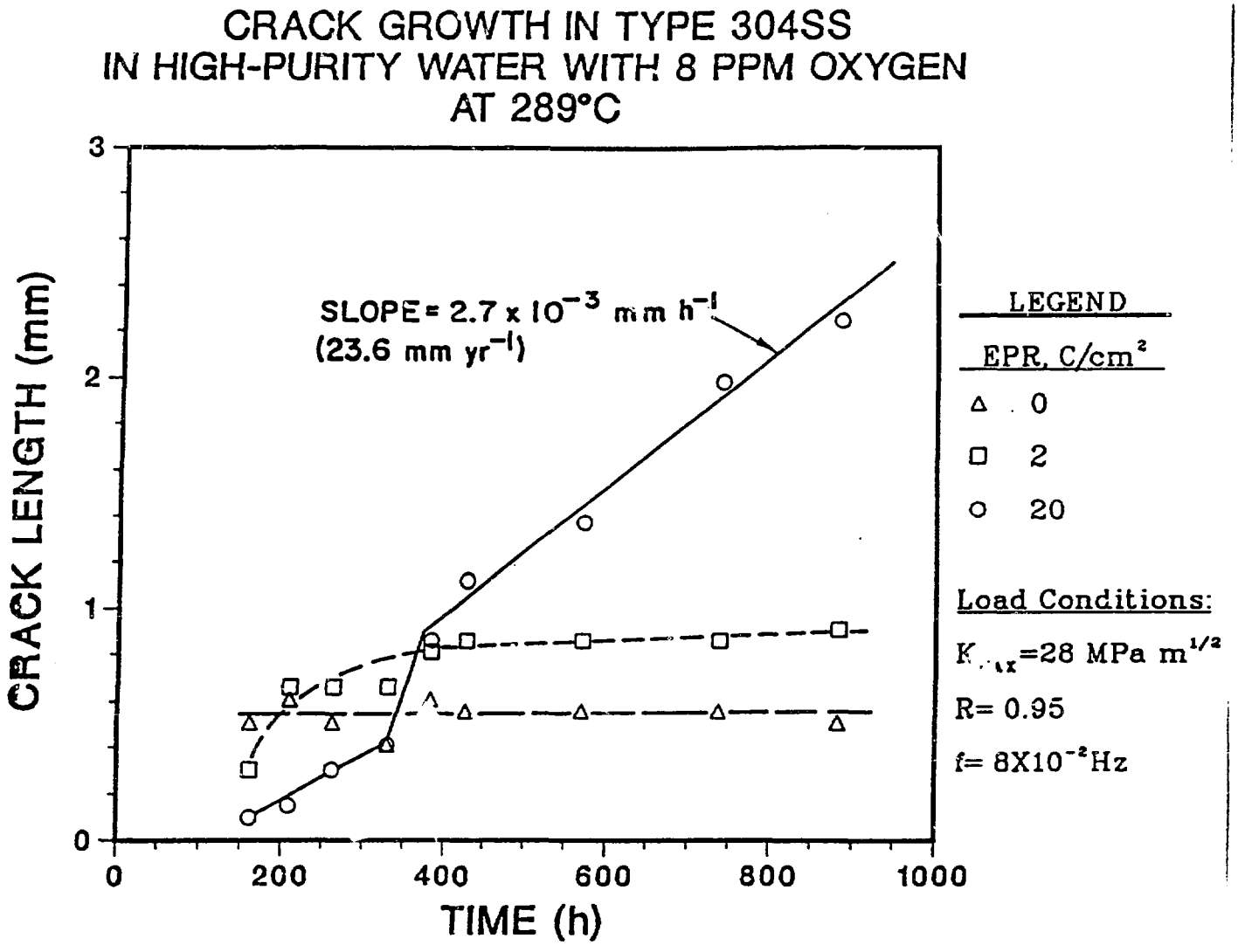

Fig. 7. Crack Length versus Time for 1TCT Specimens of Solution-annealed (EPR = 0) and Sensitized (EPR = 2 and 20 C/cm^2) Type 304 SS (Heat 30956) in 289°C Water with 8 ppm Dissolved Oxygen. The loading conditions for the positive sawtooth waveform with a slow loading time (12 s) and a rapid unloading time (1 s) are as follows: stress ratio = 0.95, K_{max} = 28 MPa·m$^{\frac{1}{2}}$, and frequency = 8 x 10^{-2} Hz.

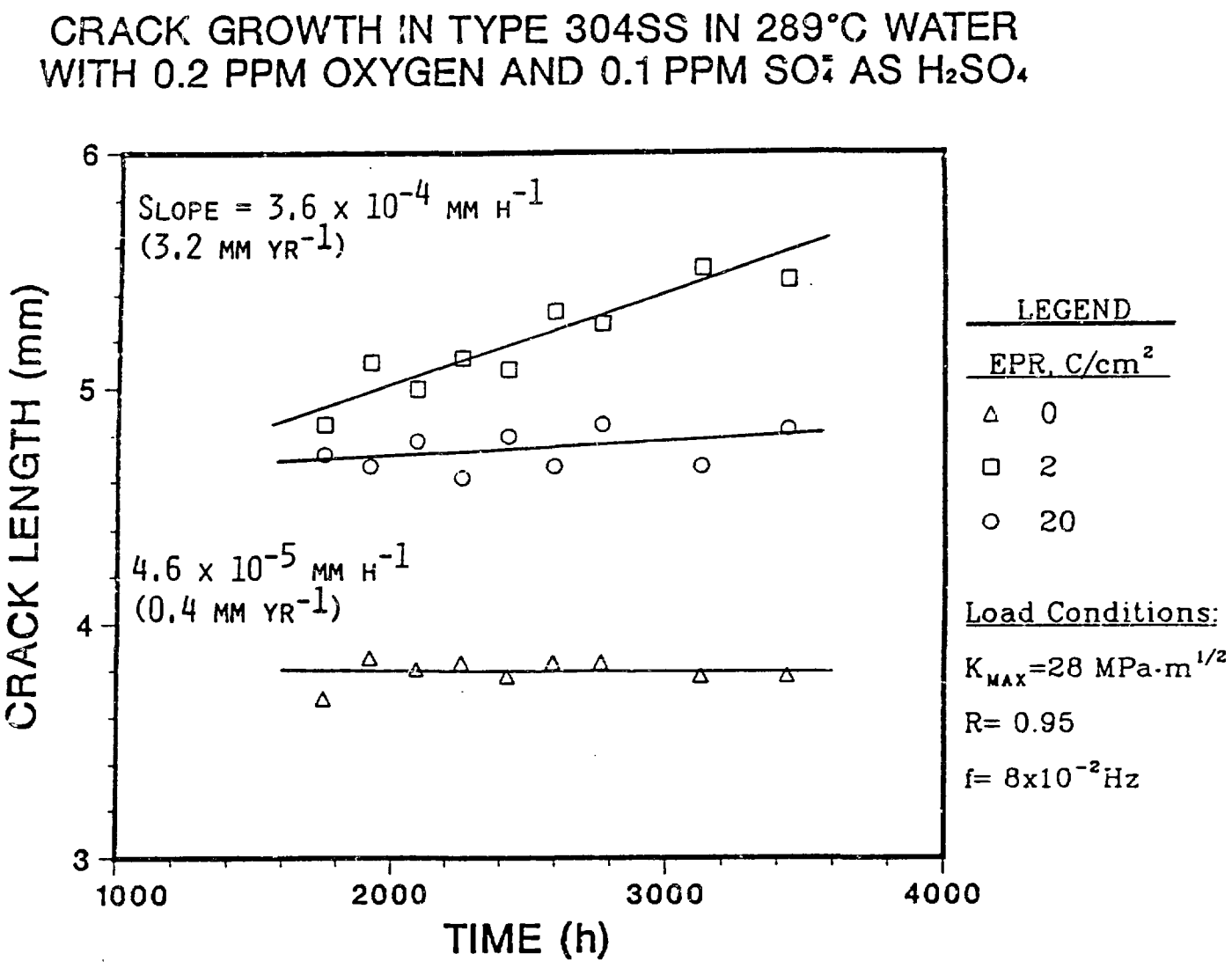

Fig. 8. Crack Length versus Time for .FCT Specimens of Solution-annealed (EPR = 0) and Sensitized (EPR = 2 and 20 C/cm^2) Type 304 SS (Heat 30956) in 289°C Water with 0.2 ppm Dissolved Oxygen and 0.1 ppm Sulfate as H_2SO_4. The loading conditions are the same as those in Fig. 7.

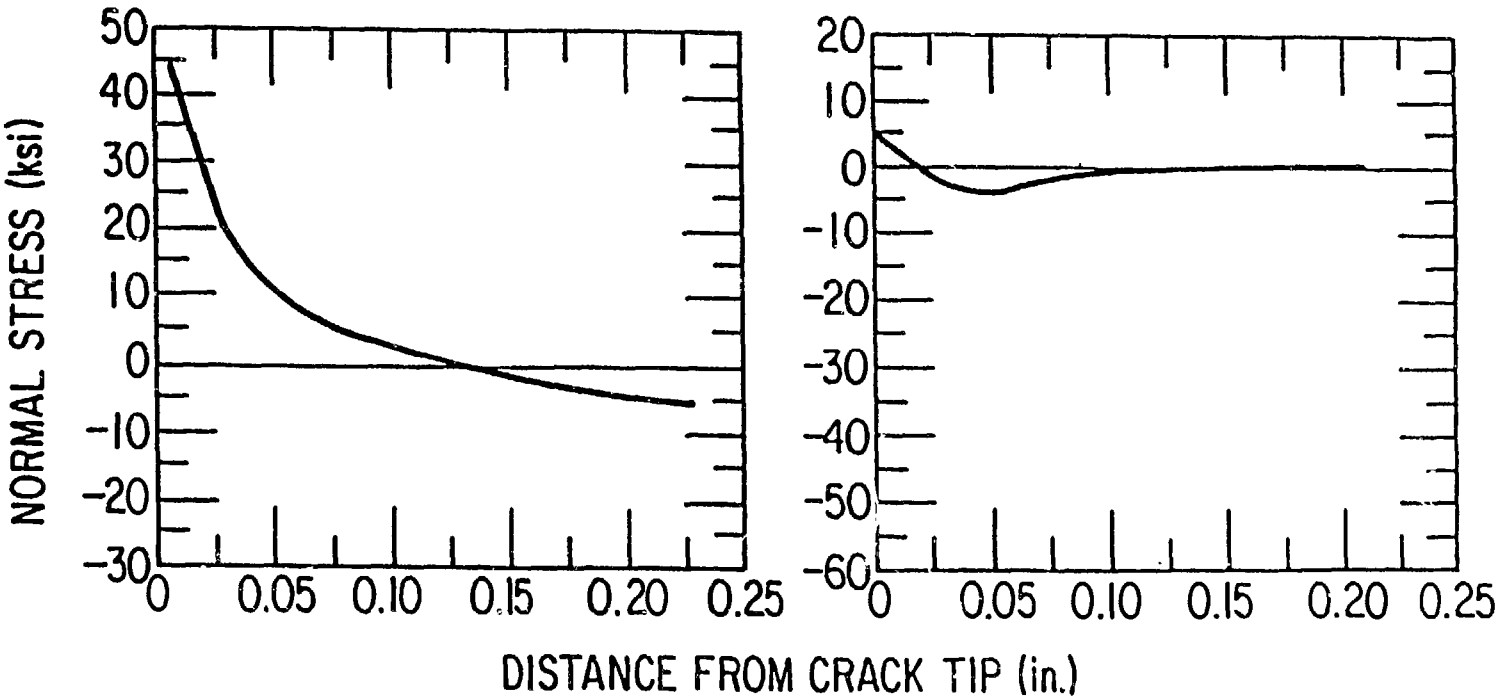

Fig. 9. Calculated Stress State Ahead of the Tip of an 8%-Throughwall Crack under an Applied Load of 103 MPa (15 ksi), Near the Heat-affected Zone of a Weldment Without IHSI (Left) and With IHSI (Right).

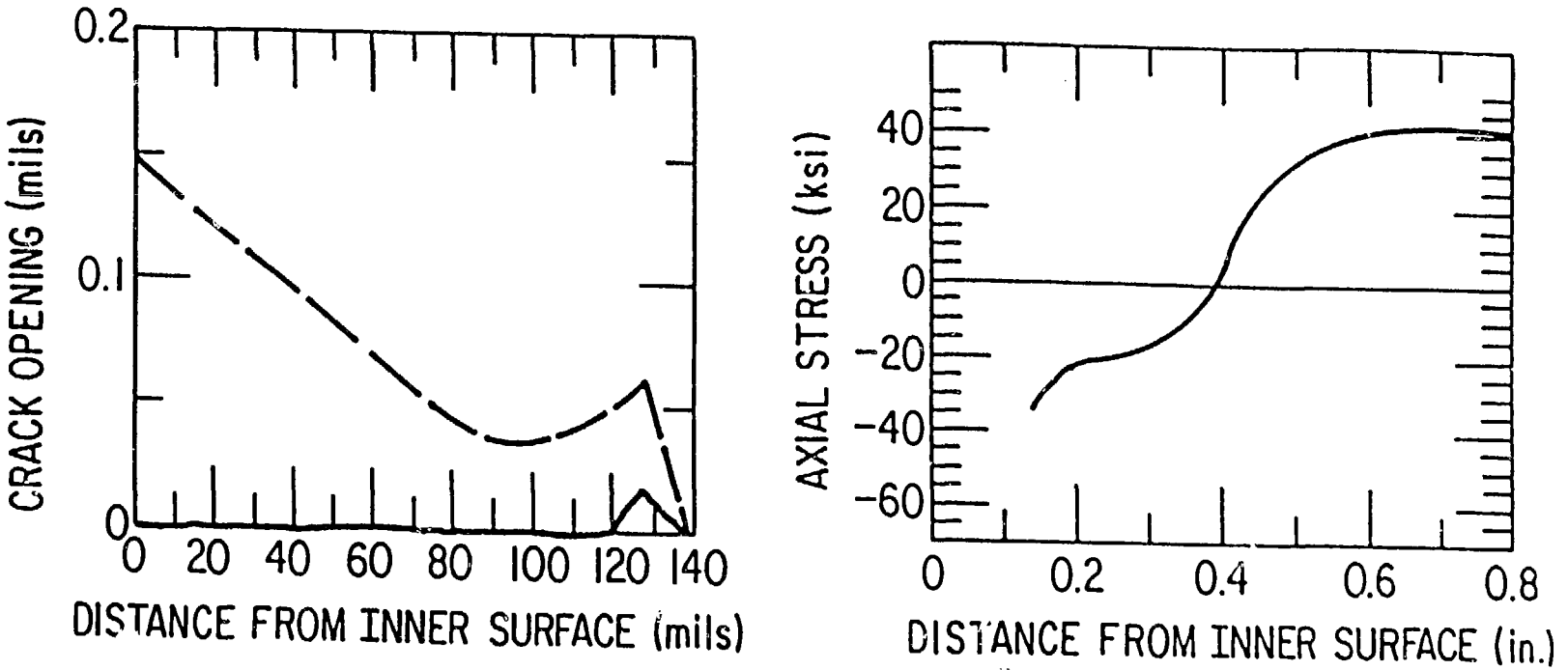

Fig. 10. (Left) Profile of Hypothetical ∿20%-Throughwall Crack Before (Dashed Line) and After Application of Weld Overlay; (Right) Calculated Stress State Ahead of the Crack Tip After the Weld Overlay Procedure, under an Applied Load of 103 MPa (15 ksi).

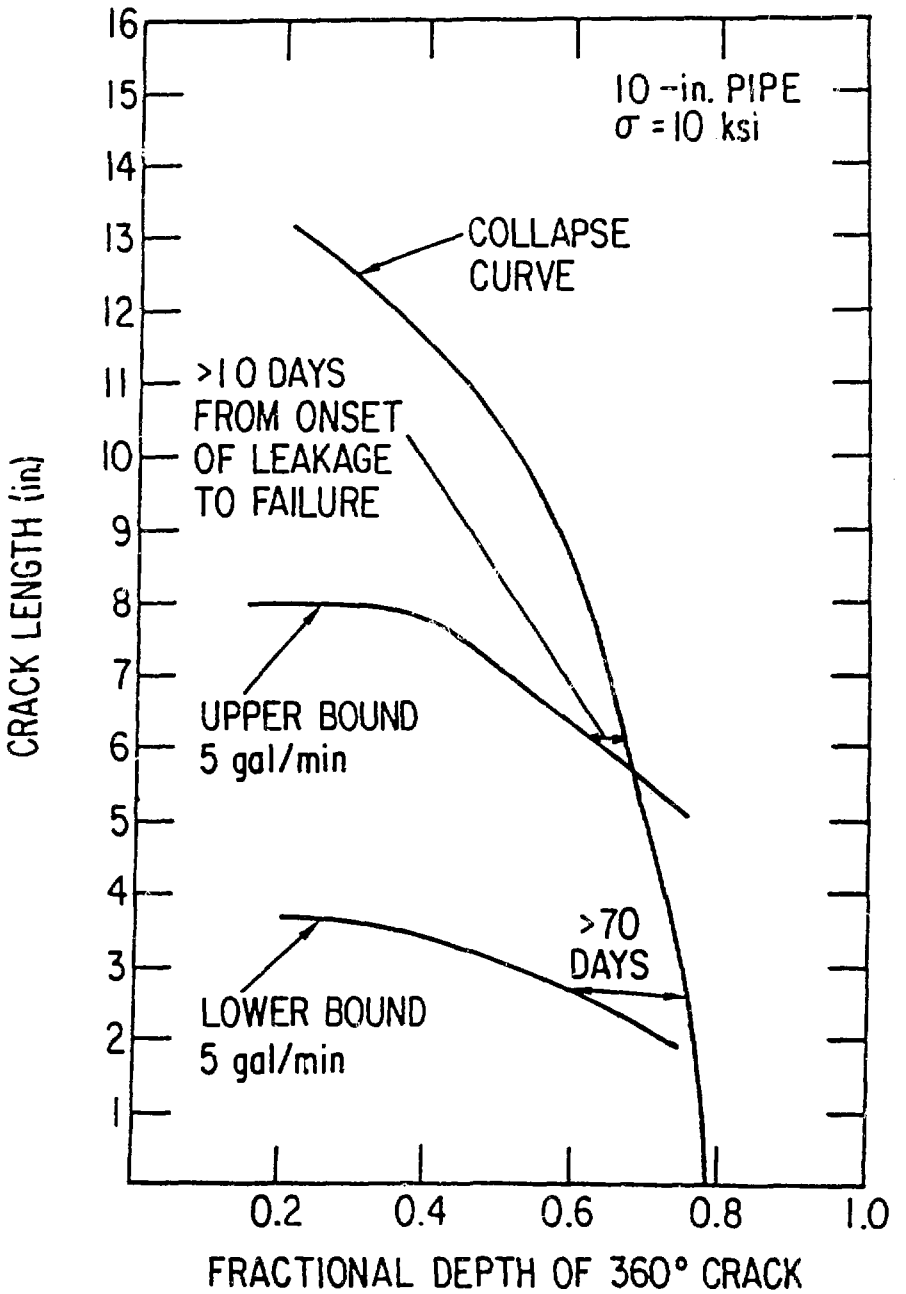

Fig. 11. Leak-Before-Break Margins for 10-in. Pipe with Combined Part-Through Circumferential Cracks and Throughwall Cracks.

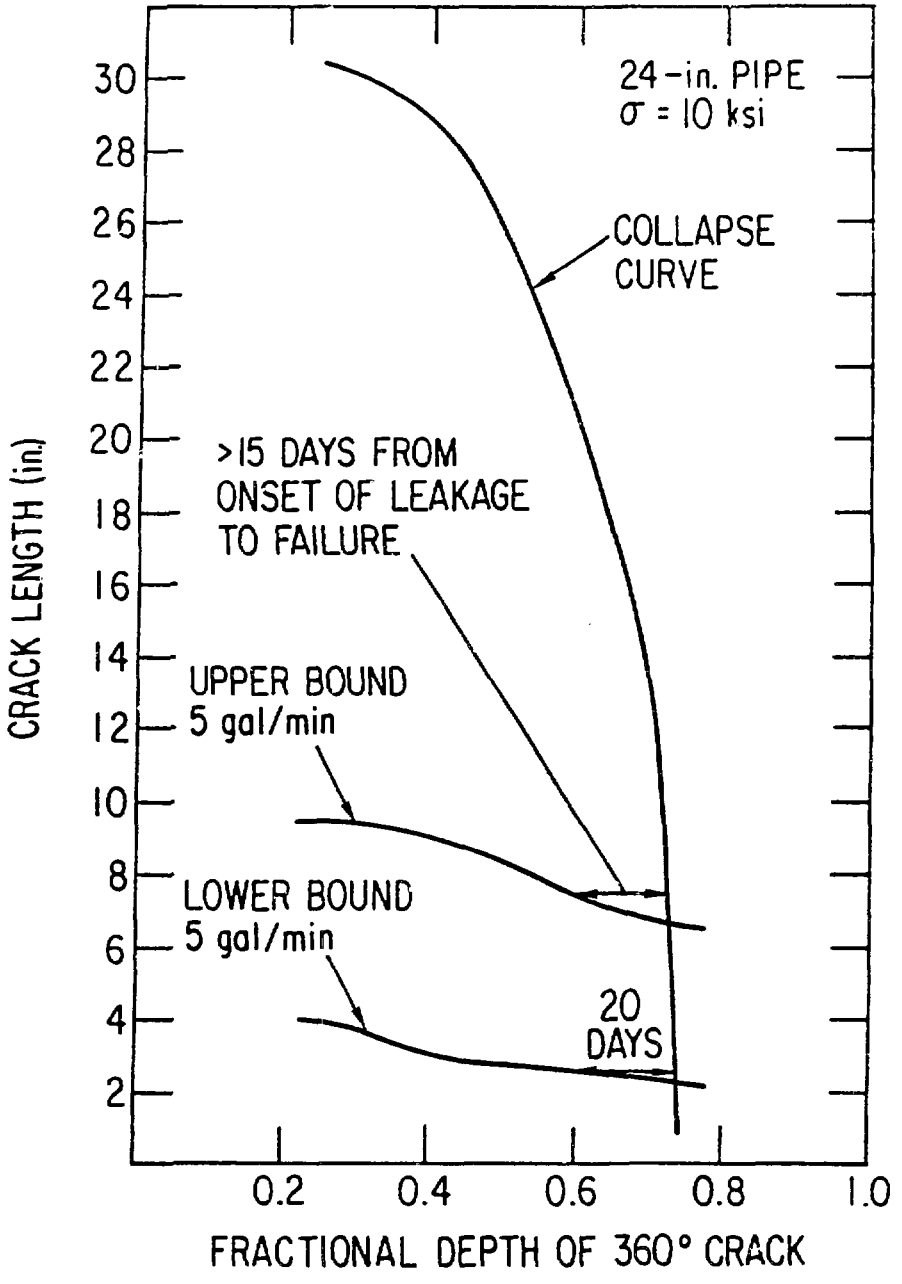

Fig. 12. Leak-Before-Break Margins for 24-in. Pipe with Combined Part-Through Circumferential Cracks and Throughwall Cracks.

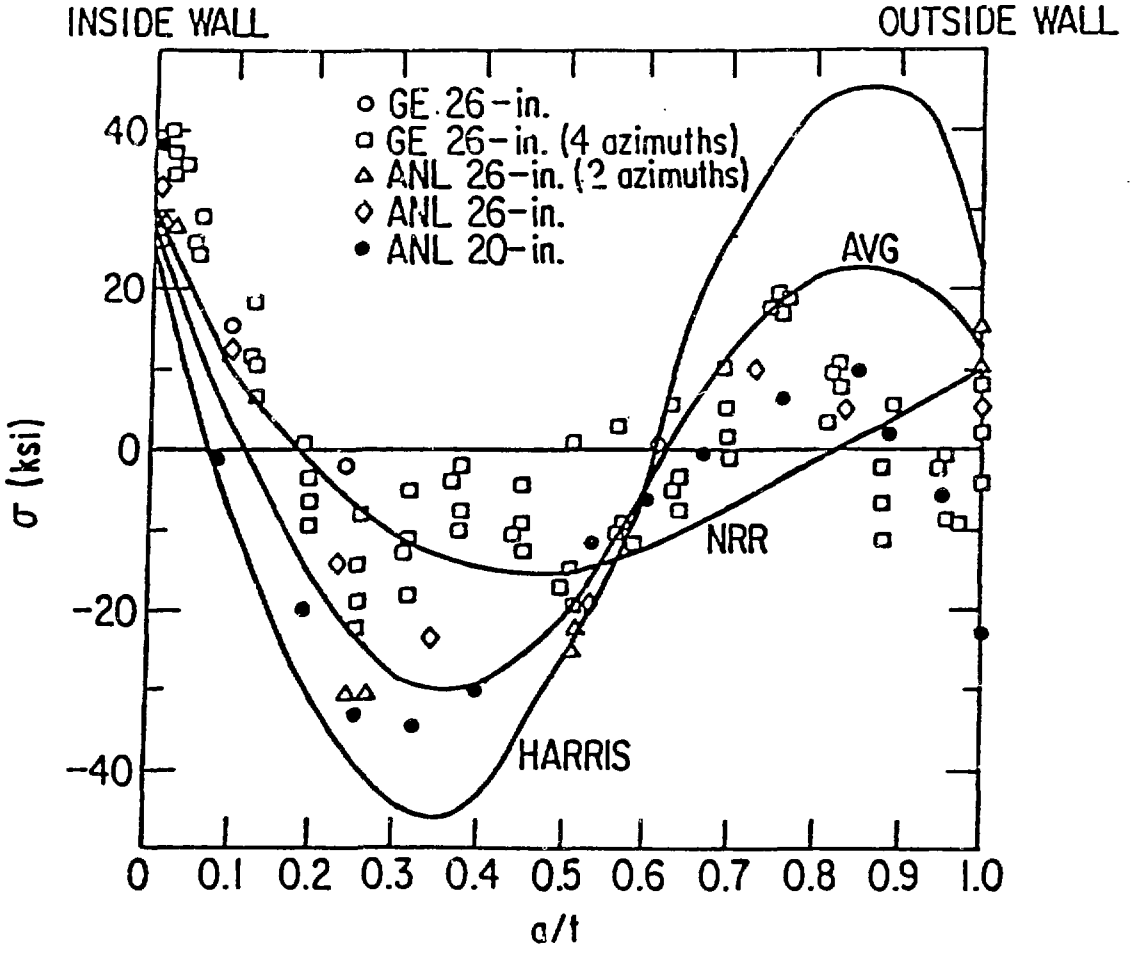

Fig. 13. Data on Throughwall Residual Stresses in Large-Diameter Pipe Weldments (from Ref. 4), and Three Analytical Representations.

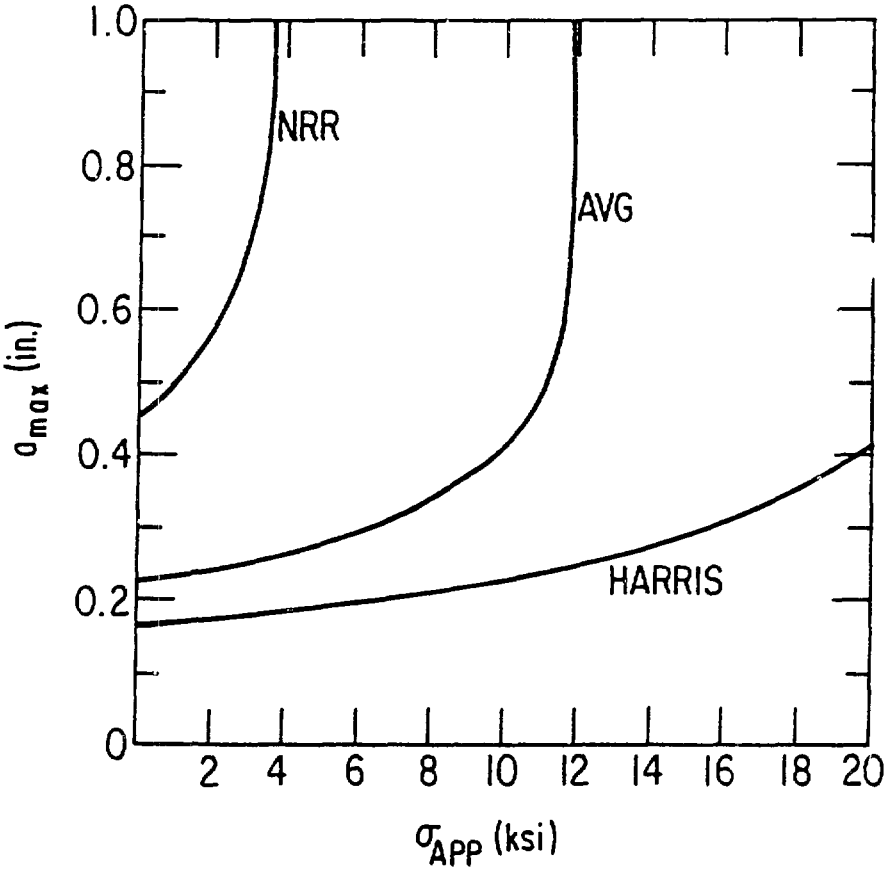

Fig. 14. Linear Elastic Fracture Mechanics Calculations of Maximum Possible IGSCC Depth vs Applied Stress for the Three Residual Stress Representations of Fig. 13.

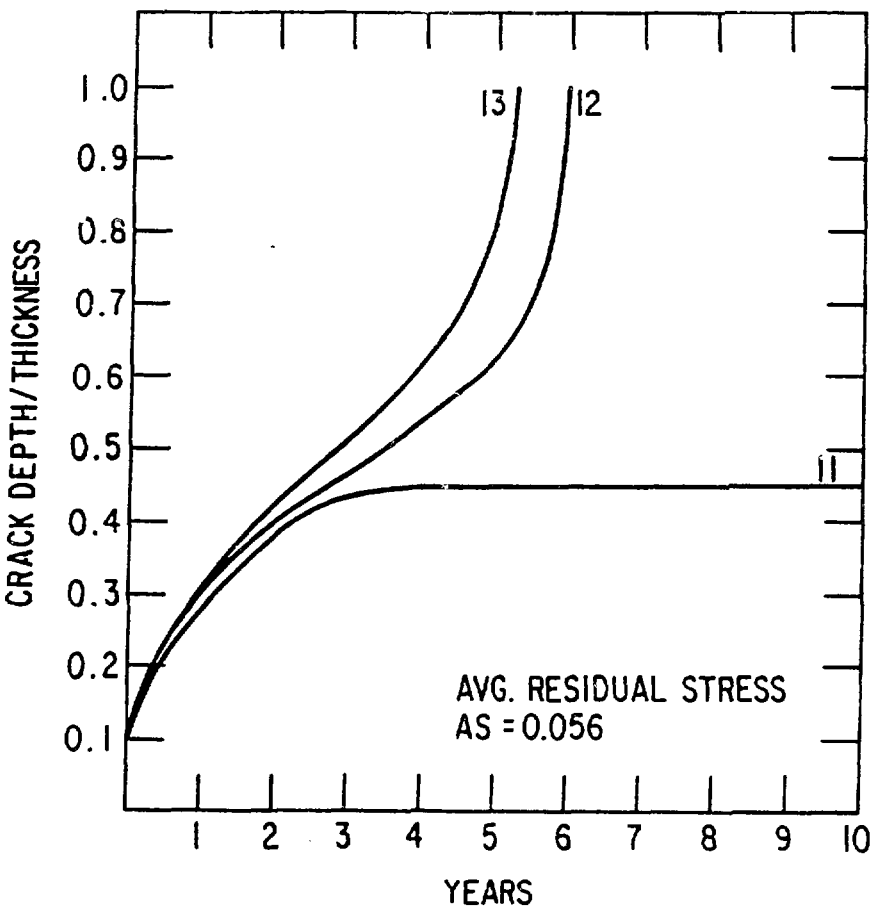

Fig. 15. Predicted Crack Depth vs Time for Three Different Levels of Applied Stress (in ksi).